Int. J. Multiphase Flow Vol. 13, No. 6, pp. 823–836, 1987
Printed in Great Britain.

0301-9322/87 $3.00 + 0.00

INVESTIGATION OF CHARGED PARTICLE TRAJECTORIES IN ELECTROSTATIC POWDER COATING SYSTEMS

M. L. ANG and P. J. LLOYD
Department of Chemical Engineering, Loughborough University of Technology, Loughborough, Leics. LE11 3TU, England

(*Received* 2 *August* 1985; *in revised form* 19 *July* 1987)

Abstract—The trajectories of charged epoxy particles, with size range 45–120 μm, in an electrostatic powder coating system were studied using a photographic technique. The results showed that the air flow from the spraying device was responsible for the initial particle transport, with increasing dominance of the electrostatic forces near the substrate mainly due to the field enhancement effect of the space charge. A computational model for calculation of the trajectories was formulated by performing a force balance of the aerodynamic and electrostatic forces involved. The accuracy of the prediction was found to depend on the initial particle exit position. Near the air jet centreline, consistent agreement was obtained, but away from it, the deviation became significant. The possible sources of this discrepancy are discussed.

1. INTRODUCTION

Electrostatic powder coating (EPC), a process utilizing similar principles to electrostatic precipitation, has been widely used in the metal finishing industry since early 1960. General descriptions of the process have been reported by Korf (1976), Harris (1976) and Wu (1976). Basically the process consists of four stages:

(a) powder charging;
(b) transport of charged particles to a conducting earthed substrate;
(c) powder deposition and adhesion;
(d) fusion of powder to form a coating.

Polymer powders are pneumatically fed from a fluidized hopper to a spray gun. Located at the gun nozzle is a pointed electrode producing a corona discharge generated by a high voltage supply (60–100 kV). Usually a negative potential is applied to produce a negative corona. The particles passing through the region are therefore charged mainly by bombardment with ions produced by the corona discharge. The combined action of the carrier air jet and the electrostatic field developed between the gun and the earthed substrate direct the charged particles towards the object to be coated. The deposited powder particles form a multi-layer until a limiting thickness is reached. Further particles arriving are rejected by an opposing field generated by the charges on the particles forming the deposited layer (Sibbett 1982). The next stage is the stoving stage, during which the deposited layer is fused and cured by baking in an oven at about 180°C to form a protective coating of uniform thickness. Oversprayed powder is collected by the recovery system and may be recycled. The first two stages are most important in determining the efficiency of the process, whilst the quality of the coatings is dependent on the two latter stages.

The deposition of particles therefore depends on the interaction of the aerodynamic and electrostatic forces during the spraying operation. The relative importance of some parameters affecting this interaction has been investigated by Golovoy (1973a, b), Singh *et al.* (1978), Abuaf & Gutfinger (1974) and Hakberg *et al.* (1983). This paper describes some results from a study of trajectories of a jet of charged particles carried out in order to achieve a better understanding of the interaction of these forces (Ang 1981). The motion of charged particles with size range 45–120 μm was investigated using a photographic technique. Particle trajectories were calculated by solving numerically the equation of motion, which was formulated by performing a force

balance. Several simple models were used to describe these fluid and electrostatic forces. The theoretical result was then compared with the experimental data. A similar study on the behaviour of a jet of charged polyethylene particles in an EPC process using larger particles (250–350 μm) was reported by Abuaf & Gutfinger (1974).

2. THEORY

2.1. Trajectory equation

Consider the flow of a suspension of particles in a fluid, under the influence of an electric field and gravity. The general vector equation is as follows:

$$m_p \frac{d\mathbf{V}_p}{dt} = C_D \pi \frac{d_p^2}{4} \frac{\rho_f}{2} |\mathbf{V}_{rel}| \mathbf{V}_{rel} + \pi \frac{d_p^3}{6} (\rho_s - \rho_f)\mathbf{g} + \sum \mathbf{F}_e; \quad [1]$$

where $\mathbf{V}_p$ is the absolute particle velocity; ρ_s and ρ_f are the densities of solid and fluid, respectively; $\mathbf{g}$ is the gravitational constant; C_D is the drag coefficient; m_p is the particle mass; d_p is the particle diameter; $\mathbf{F}_e$ is the electrical field force; and $\mathbf{V}_{rel}$ is the local fluid velocity relative to the particle velocity.

For a particle at a point O (x, y) in a two-dimensional flow field, as shown in figure 1,

$$\mathbf{V}_p = \mathbf{V} - \mathbf{V}_{rel}, \quad [2]$$

$$\dot{x} = \frac{dx}{dt} = U - V_{rel\,x}, \quad [3]$$

$$\dot{y} = \frac{dy}{dt} = V - V_{rel\,y} \quad [4]$$

and

$$|\mathbf{V}_{rel}| = V_{rel}[(U - \dot{x})^2 + (V - \dot{y})^2]^{\frac{1}{2}}, \quad [5]$$

where $\mathbf{V}$ is the fluid velocity vector, U and V are the x and y components of the fluid velocity and $V_{rel\,x}$ and $V_{rel\,y}$ are the x and y components of the particle relative velocity, respectively.

To solve [1], the following assumptions are made:

(a) the particles are spherical and monosized;
(b) the suspension is dilute and particle/particle interaction can be ignored;
(c) each particle is considered a point mass and does not affect the fluid flow pattern and the electric field.

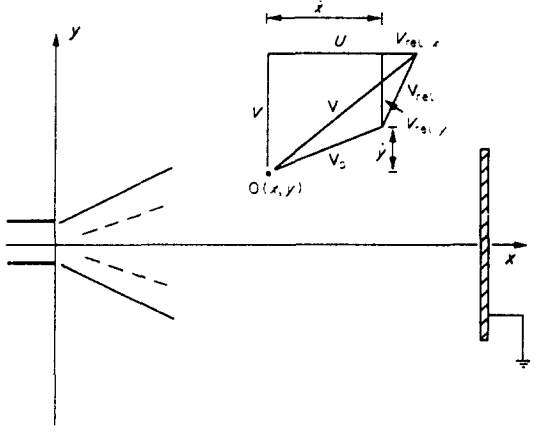

Figure 1. Schematic representation of the flow field.

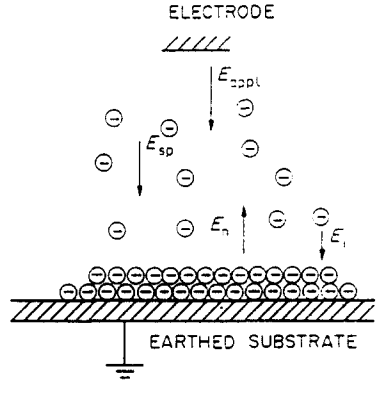

Figure 2. The electrical fields of the EPC process: E_{appl} = applied field; E_i = image field of a charged particle; E_n = field due to the deposited layer; E_{sp} = space charge field of charged particles and ions.

Resolving [1] in the x and y directions:

$$m_p \frac{d^2x}{dt^2} = C_D \pi \frac{d_p^2}{4} \frac{\rho_f}{2} V_{rel}\left(U - \frac{dx}{dt}\right) + \sum F_{e,x} \quad [6]$$

and

$$m_p \frac{d^2y}{dt^2} = C_D \pi \frac{d_p^2}{4} \frac{\rho_f}{2} V_{rel}\left(V - \frac{dy}{dt}\right) + \sum F_{e,y} - (m_p - m_f)g; \quad [7]$$

$F_{e,x}$ and $F_{e,y}$ are the components of the electrical field forces.

The drag coefficient C_D for a particle depends primarily on the Reynolds number based on the fluid particle relative velocity and is given by

$$Re_p = \frac{\rho_s |V_{rel}| d_p}{\mu}, \quad [8]$$

where μ is the fluid viscosity. Here, the drag coefficient is calculated using

$$C_D = \left(\frac{24}{Re_p}\right)(1.0 + 0.15\, Re_p^{0.687}), \quad [9]$$

which is for $Re_p < 1000$ (Wallis 1969).

The numerical integration of [6] and [7] was performed using a fourth-order Runge–Kutta technique on an ICL 1904A computer. To initiate the calculation, a particle was assigned a specific starting position and initial particle velocity components. These initial values were obtained from experimental data.

2.2. The electrical forces

In the EPC process, the role of the corona electrode is dual purpose. It produces the ions required for the particle charging and it also determines the deposition field between the electrode and the substrate. In calculating the net electrical force acting on a particle, one must take into account the electric fields shown in figure 2, viz. the space charge field E_{sp} due to the charged particles and ions, the applied field E_{appl} produced by the electrode system, the image field E_i and the field E_n due to a deposited layer of particles. The electrical force acting on a charged particle is given by

$$\sum \mathbf{F}_e = qE', \quad [10]$$

where E' is the local net electric field and q is the charge on the particle.

Particle charging occurs between the electrode and the substrate by ion bombardment charging and ion diffusion charging. Only ion bombardment charging is considered since it is the dominant charging mechanism in the vicinity of the charging electrode where there is an intense corona field. Also diffusion charging becomes predominant only for small particles, typically below 0.5 μm (White 1963). The value of q used in the calculation is approximated by that of saturation or limiting charge, given by

$$q = 3\pi\left(\frac{\epsilon}{\epsilon + 2}\right)\epsilon_0 d_p^2 E_0, \quad [11]$$

where ϵ_0 is the permittivity of free space and E_0 is the charging field strength. For a polymer particle, the relative permittivity ϵ is of the order of 2.0. To attain this saturation value, the residence time for a particle in a charging zone with field E_0 is usually of the order of 10^{-3}–10^{-4} s (White 1963; Bright & Bassett 1975). In this study of particle trajectories, for particles emerging with a measured maximum velocity of about 5 m/s, the calculated residence time in the charging zone was typically 10^{-3} s with longer residence time for those emerging with lower velocities. Further charging would also result as the particles streamed towards the earthed substrate.

With a given space charge density ρ, the differential equation of the field is described by Poisson's equation which governs all electrostatic phenomena:

$$\nabla^2 v = -\frac{\rho}{\epsilon_0}, \quad [12]$$

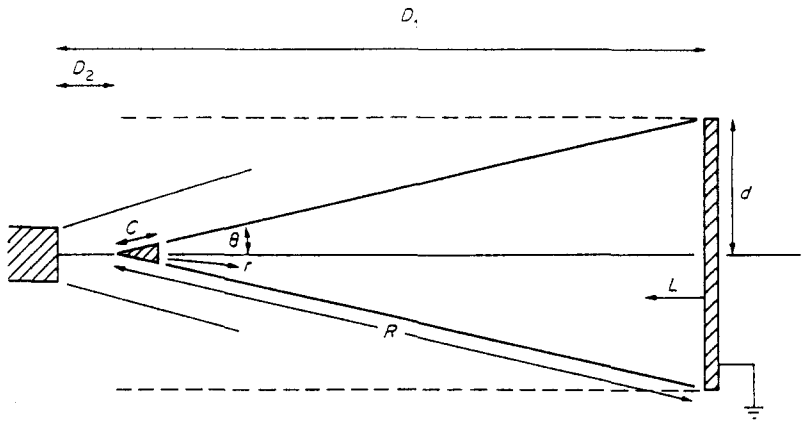

Figure 3. The electrostatic field model. Image force considered in $D_2 < x < D_1$, $y = \pm d$. Conical shell in which other electrostatic forces are considered: $D_2 < x < D_1$, $y = \pm \tan\theta(x - D_2)$.

where v is the potential. The electric field E is related to the potential by

$$E = -\nabla v. \qquad [13]$$

Equation [12] cannot be solved easily for an EPC process since this is a three-dimensional problem and is further complicated by the little known nature of the space charge density distribution. There is also the uncertainty, in the boundary conditions at the electrode due to the complicated nature of the corona discharge phenomena. Based on the model of Wu (1976) and using a point–plane configuration as shown in figure 3, a simple model was derived by solving the one-dimensional Poisson's equation assuming constant charge density (Ang 1981). The solution of field intensity $E(r)$ is given by

$$E(r) = \left(\frac{\rho}{3\epsilon_0}\right) r + \left[\frac{(v_a - v_p) - \dfrac{\rho}{6\epsilon_0}(R^2 - C^2)}{\left(\dfrac{1}{C} - \dfrac{1}{R}\right)}\right] \frac{1}{r^2} = \alpha r - \frac{\beta}{r^2}, \qquad [14]$$

where r is the radial distance, v_a is the applied potential, v_p is the potential of deposited layer, R is the separation distance and C is the radius of the corona region. The potential $v(r)$ is described by

$$v(r) = v_a + \frac{\alpha}{2}(C^2 - r^2) + \beta\left(\frac{1}{C} - \frac{1}{r}\right). \qquad [15]$$

Without the space charge, i.e. $\rho = 0$, [14] and [15] reduce to

$$E(r) = \frac{RC(v_a - v_p)}{r^2(R - C)} \qquad [16]$$

and

$$v(r) = \frac{v_a C(r - R) + v_p R(C - r)}{r(C - R)}. \qquad [17]$$

By denoting the field intensity with and without space charge by E_{wsp} and E_p respectively, [14] and [15] are combined to produce:

$$E_{wsp} = \left[\frac{(v_a - v_p) - \dfrac{\rho}{6\epsilon_0}(R^2 - C^2)}{(R - C)}\right] \frac{CR}{r^2} + \frac{\rho r}{3\epsilon_0} = E_p - \frac{\rho CR(R^2 - C^2)}{6\epsilon_0 r^2(R - C)} + \frac{\rho r}{3\epsilon_0} = E_p + \delta, \qquad [18]$$

where

$$\delta = \delta_1 + \delta_2,$$

$$\delta_1 = -\frac{\rho CR(R^2 - C^2)}{6\epsilon_0 r^2(R - C)}$$

and

$$\delta_2 = \frac{\rho r}{3\epsilon_0};$$

δ is a parameter describing the contribution of the space charge effect to the overall field distribution. When r is small, i.e. near the corona point, δ is negative since $\delta_1 \gg \delta_2$. Near the substrate, δ is positive since δ_2 is predominant. Therefore:

$$\delta < 0 \quad \text{when} \quad r \to C; \quad \delta_1 \gg \delta_2;$$

and

$$\delta > 0 \quad \text{when} \quad r \to R; \quad \delta_1 \ll \delta_2.$$

In the vicinity of the corona electrode the electric field suffers a suppression by a value of δ_1, but near the earthed electrode it is increased by δ_2.

From [14], if

$$\frac{\beta}{r^2} \gg \alpha r$$

it follows that the relationship

$$(v_a - v_p) \gg \frac{\rho}{6\epsilon_0}(R^2 - C^2) \qquad [19]$$

is true. If this condition is satisfied, the effect of space charge density can be neglected. The magnitude of

$$\left[(v_a - v_p) - \frac{\rho}{6\epsilon_0}(R^2 - C^2)\right]$$

can be used as a criterion to gauge the significance of the space charge contribution.

This simple model described by [14] was compared with experimental data from measurements of the electric field distribution for several point-plane electrode systems (Corbett 1972). Figure 4 shows an example of a comparison. Generally the trend is correctly predicted, although before the minima the field intensity decay is more aptly described by r^{-1} type behaviour than by r^{-2} type. Further data are presented in Ang (1981). The field equation is resolved to give rise to the two field components, E_x and E_y, for solving the trajectory equations.

The image force $\mathbf{F}_i$ on a charged particle at a distance L from the substrate is expressed by

$$\mathbf{F}_i = \frac{q^2}{4\pi\epsilon_0 L^2} \qquad [20]$$

This is one of the major forces responsible for powder adhesion in EPC. The magnitude of this force is, however, insignificant when compared to the applied field forces in the trajectory calculation.

The presence of corona discharge also causes a secondary flow, often known as electric wind or corona wind (Yamamoto & Velkoff 1981). The movement of ions under the influence of an electric field transfers momentum to the carrier medium by friction and results in this further flow. The mechanical force produced is appreciable only if unipolar ions are present. The published experimental data, mainly on the electrostatic precipitation process, have shown great variation

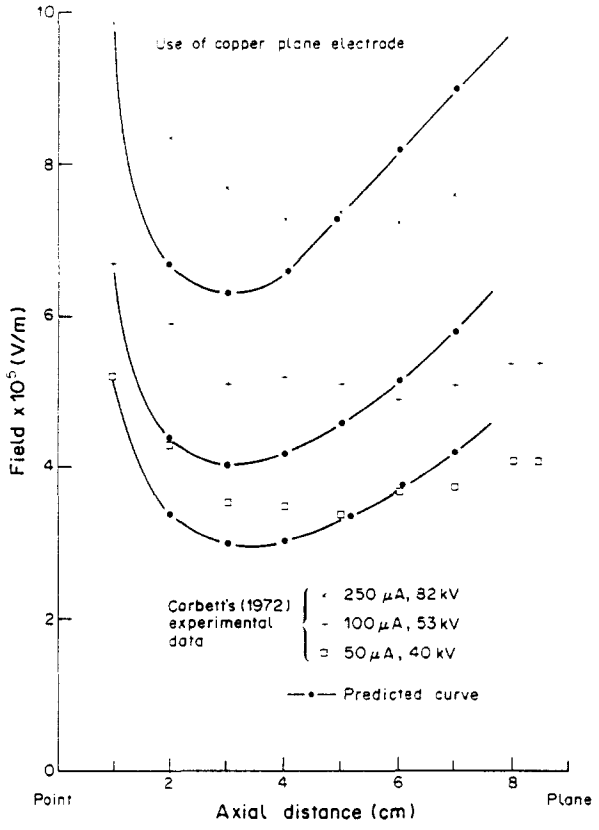

Figure 4. Comparison of field intensity distribution data.

in magnitude depending on experimental conditions. Under typical EPC conditions, the corona wind velocity is of the order of 1 m/s (Singh *et al.* 1978). This velocity component V_c is approximated by

$$V_c = \left(\frac{\epsilon_0}{\rho_f}\right)^{\frac{1}{2}} E(r). \qquad [21]$$

For the present calculation, with $E_0 = 3 \times 10^5$ V/m in the corona region, V_c assumed a maximum value of 0.81 m/s.

In EPC, the mechanism responsible for the "self-limiting" phenomenon in the growth behaviour of the deposited powder layer is back ionization (Cross & Bassett 1974). Due to the high resistivity of the coating powder (typically 10^{14}–10^{16} Ωm), the deposited particles do not discharge quickly. The potential and the electric field increase with the growth of the layer until eventually the breakdown field strength is reached. This results in a counterflow of ions opposite in sign to those from the gun, discharging and turning away oncoming powder particles. The surface potential v_p of a charged powder layer and the attainment of critical coating thickness have been investigated and modelled by Hardy (1974), Wu (1976) and Sibbett (1982). However in this study, the value of v_p was neglected since a very dilute suspension was used and in the experiments particle build-up on the substrate was not permitted.

To solve the trajectory equations, several assumptions were made:

(a) the electrical forces were confined in a conical configuration determined by the point corona electrode and the substrate as in figure 3;
(b) the earthed substrate acted as a perfect sink, i.e. $v_p = 0$;
(c) the corona wind effect and the particle image force were considered only in [6].

2.3. The aerodynamic forces

The air flow field in an EPC system is the resultant of two separate air flows: one due to the

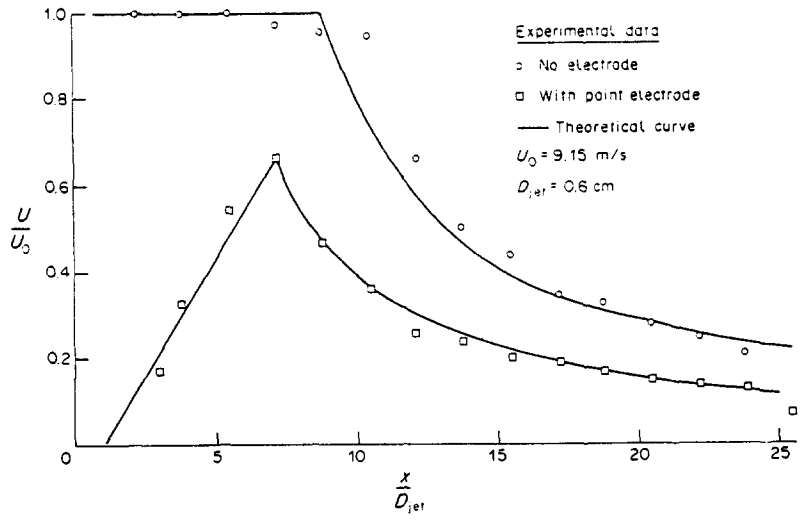

Figure 5. Variation of the centreline velocity of a round jet.

powder feed system via the powder spray gun, and the other a secondary flow due to the powder recovery system. There is great variation in the design of industrial hand-spraying devices which generally give an emerging air velocity of the order of 8–15 m/s. In this trajectory study a simplified system was used, involving an air jet issuing from a nozzle with an attached electrode. Using a hot-wire anemometer, air flow from the nozzle was measured with and without the electrode. Figure 5 shows the effect of the electrode in reducing the jet centreline velocity of a round jet. Between the fully developed jet region and the nozzle, the potential core was replaced by a region of increasing velocity. For the trajectory calculation, the air velocity in this region was described by a correlation based on the air flow measurement. The fully developed jet region was found to be reasonably approximated by Tollmien's solution for an axisymmetric jet (Abramovich 1963). The calculated velocity values and the jet widths, however, tended to be overestimated.

In EPC, the secondary air flow due to the filtration system is about 0.3 m/s. To modify significantly the air flow from the spray gun and thus affect the particle trajectory, the velocity of this secondary stream needs to be at least of the order of 1.5 m/s. This flow was therefore neglected in the trajectory calculation.

3. EXPERIMENTAL INVESTIGATION OF PARTICLE TRAJECTORIES

In this experimental study of particle trajectories chronophotography, i.e. photography using interrupted illumination was used. The principle of operation is as follows. When the field of view of the fluid containing suspended particles is subjected to interrupted illumination, depending upon their positions, successive images are recorded on a photographic plate. The velocities of the particles can be calculated from the distance travelled by the particles and the time interval between consecutive bursts of illumination. The position of emergence of a particle and its initial velocity can be determined directly from the enlarged photographs. The illumination was provided by a high power stroboscope. Abuaf & Gutfinger (1971) achieved this light interruption by using a sectored wheel which rotated across an incident light beam.

Figure 6 shows schematically the apparatus, which basically consisted of:

(a) the spray booth;
(b) the illumination and photographic system;
(c) the powder spraying and charging system.

Compressed air after passing through a clean air filter and a silica gel drying column, flowed through a rotameter and was issued as a free jet at the nozzle. The rotameter was calibrated using a gas meter and the calibration graph enabled direct reading of the air exit velocity. The exit velocities of between 6.80–10.60 m/s were also checked using a hot-wire anemometer. The particle

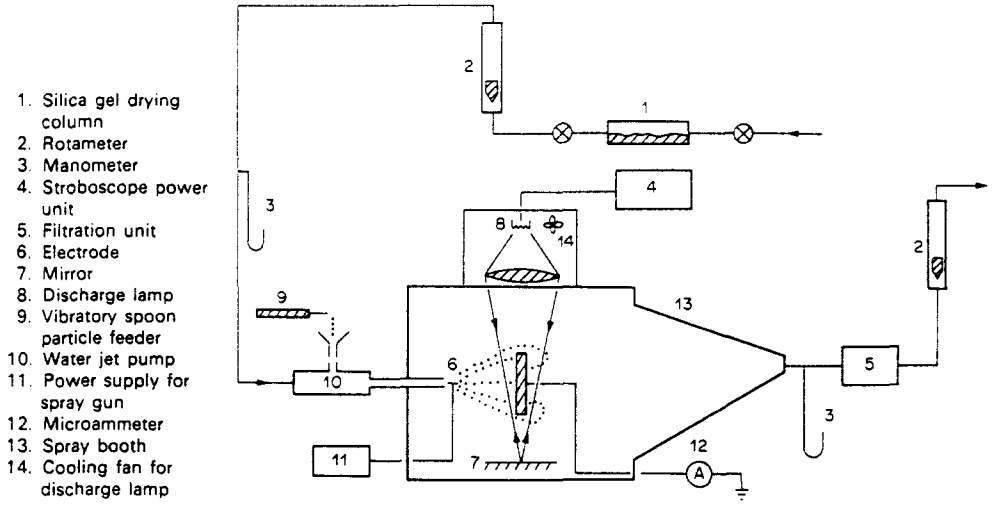

Figure 6. Schematic of the experimental setup.

feeder consisted of a vibratory spoon feeder and a water jet pump. This arrangement enabled only a few particles to be dropped and entrained in the air stream at any instant and the vibratory spoon feeder could also maintain a steady flow of particles. Epoxy particles of three sieved size ranges: 45–53, 75–90 and 105–125 μm, were used in the experiments. For this experimental setup, determined mainly by the spraying distance, the size range of 45–53 μm was found to be the smallest to yield acceptable photographic records of trajectories. Trajectories for smaller particles could be obtained if the field of view could be reduced.

The interrupted illumination was provided by a high-power, high-speed, short-duration stroboscope, capable of providing between 400–16,000 flashes/s. Flashing rates of 400–600 flashes/s were found to be adequate and they were precisely set using a digital counter. To obtain maximum illumination, a projector lens was used for focusing the light on the experimental region. A Yashica TL Electro X camera, equipped with a 35 mm f/2.8 Zeiss Flektogen lens with a 2 × teleconvertor, was used for the initial photographic work. The experiments progressed later with a Nikkon FD2 camera with a 35 mm f/2.0 Nikkor lens and a 2 × teleconvertor. By photographing a graticule used for calibration, the depth of field was determined to be 1–1.5 cm for the two photographic systems. Many preliminary experiments were conducted with different camera–lens combinations and object–camera distances to produce this sytem with an acceptable field of view which also afforded a high resolution of the particle trajectories.

The power generator which provided the source of high tension was part of an Aerostyle EPC system, capable of a maximum output of 80–90 V at 50 μA. Polarity of the output was negative. The potential was calibrated using 10 resistances of 10 GΩ connected in series. The results presented in this paper were from experiments using a point corona electrode made of a short 3 mm needle although a conical electrode was also used in other experiments (Ang 1981). The objects to be coated were 5.3 × 5.3 cm stainless-steel plates.

For tracing of the particle trajectories, the negatives from the experiments were projected onto a wall using an Elmo slide projector. The magnification of the experimental area was 2.6×. The nozzle, forming the origin of the coordinate system, and the target plate were drawn together with the trajectories to define the spatial relationship of the system. Several negatives were superimposed to produce an overall trajectory picture for a particular set of experimental conditions. Only complete trajectories which were in focus were considered in the analysis. The traced trajectories were processed using a Vanguard digital X–Y data reader which enabled the coordinates of the particles to be determined accurately.

4. RESULTS AND DISCUSSION

Some examples of comparison of experimental trajectories and the corresponding predicted values are presented in figures 8–12 for particles of three size fractions (45–53, 75–90 and

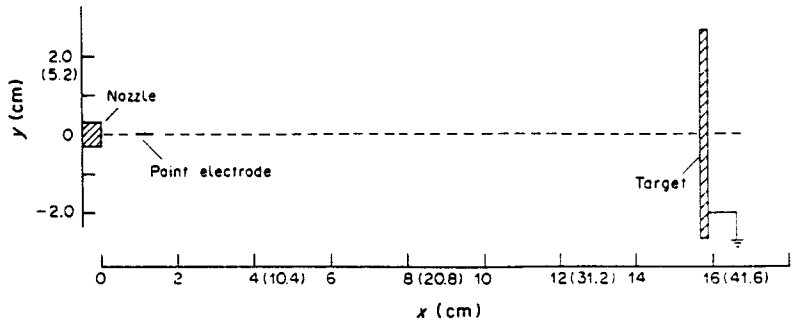

Figure 7. Experimental configuration. Figures in parentheses are the magnified scales used in figures 8–12.

105–125 μm). These experimental trajectories were actual traced results showing the particle position for the duration of the interrupted illumination. Figure 7 defines the configuration of the experimental setup and it also shows that actual experimental scale and the magnified scale used in the processing of the recorded trajectories. Figures 8–12 use the magnified scale. Each trajectory was compared with computed values with and without the consideration of the electric fields in order to assess the contribution of these electrical forces.

The comparison is generally consistent, showing that the presence of an electric field effectively helped to overcome the gravitational effect and confined the particles within the air stream. Agreement is reasonable for particles emerging near the jet centreline but away from it there is marked deviation in the comparison. This disagreement becomes more severe with increasing angle of emergence of the particles, e.g. T1 in figures 8 and 9, and T4 in figure 11 (T denotes trajectory). These particles were deposited although the calculations indicated otherwise. Several factors could contribute to this discrepancy.

Above the jet centreline, the particle giving T1 in figure 8 is seen to be overcome by the gravitational force and resulted in re-entrainment in the air stream. It is then subjected to the combined effect of the electrical field and fluid forces and thus deposited. For a particle trajectory with a wide positive angle of emergence, it is clear that the particle is experiencing a higher drag than calculated which results in a more rapid decay of particle velocity. Other experiments without

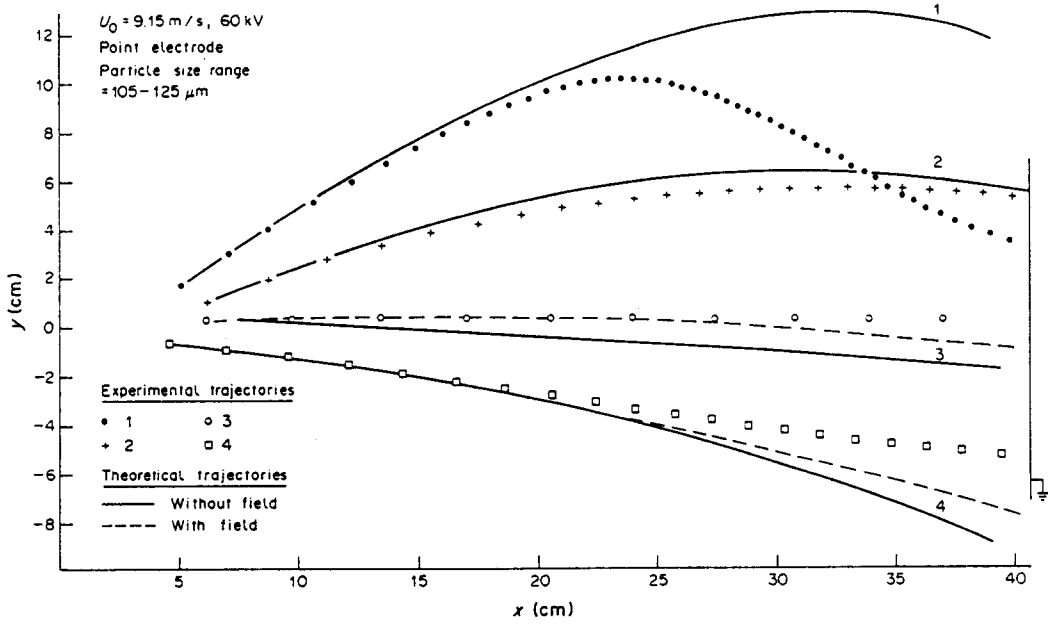

Figure 8. Comparison between experimental and theoretical trajectories.

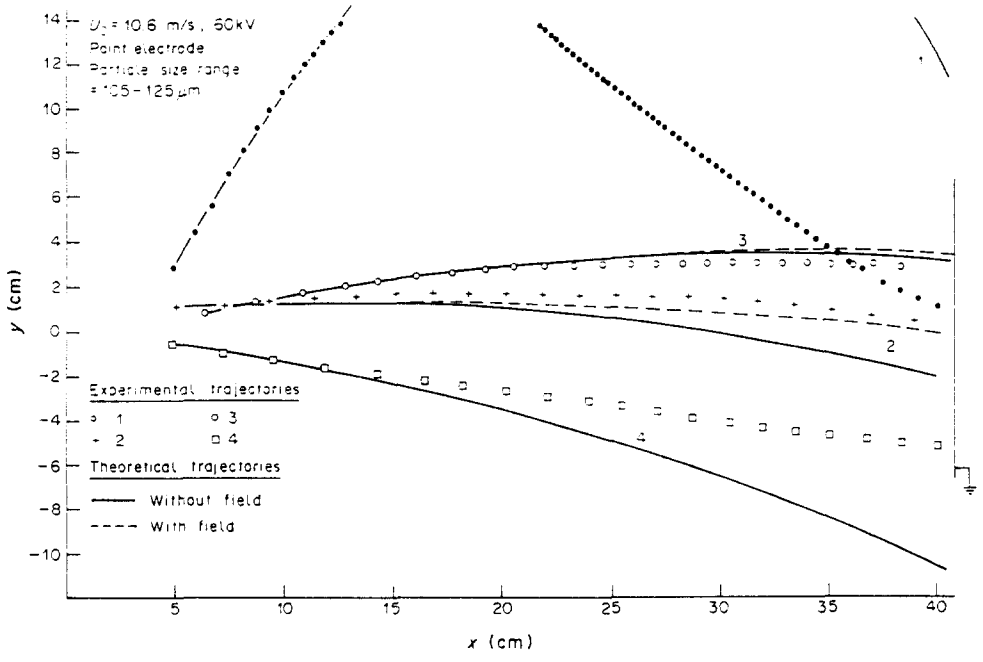

Figure 9. Comparison between experimental and theoretical trajectories.

the applied field similarly displayed this behaviour of rapid velocity decay and re-entrainment. Air measurements also confirmed negligible air flow outside the conical geometry. This suggests the inadequacy of using [9] which is strictly applicable to spherical particles to deal with angular particles. The drag coefficient would further have to account for the tumbling and rotational motion evidently displayed in trajectories of larger particles (Ang 1981). This anomaly could be verified by performing further calculations using more appropriate particle drag correlations.

In the computational scheme, the electrostatic forces were assumed to be confined within a cone. The boundary of this cone was defined by the positions of the corona electrode and the earthed plate. If particles were outside this boundary, they were assumed to be unaffected by any electrostatic force. In the case of particles emerging below the centreline and outside the cone (e.g. T4 in figure 9), these trajectories however showed clearly the presence of electrostatic forces sufficient to overcome the gravitational effect and thus the particles maintained the deposition

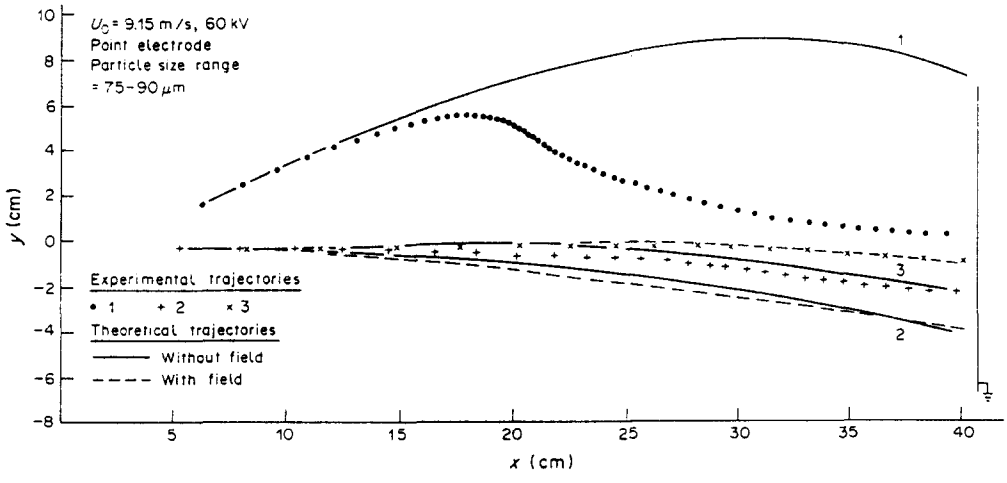

Figure 10. Comparison between experimental and theoretical trajectories.

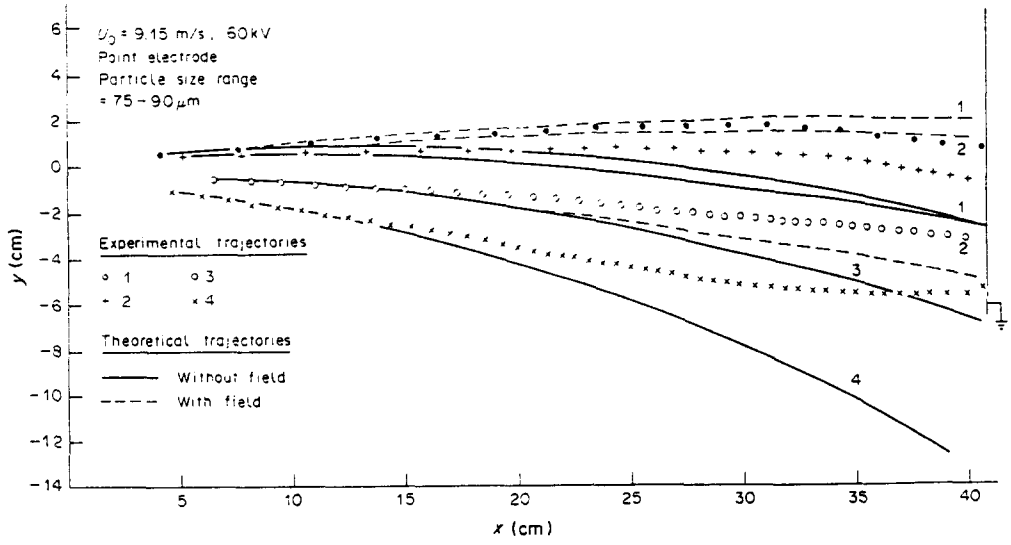

Figure 11. Comparison between experimental and theoretical trajectories.

course. Other recorded trajectories not included in this paper, for particles with even wider angle of emergence, showed attempt by the electrostatic forces to "lift" the charged particles against the gravitational forces. This suggests either the presence of unconsidered electrostatic forces or a larger field boundary than that prescribed by the conical shell. One possible explanation may be due to the edge effect of the object. It has been confirmed in experiments by Ting (1978) that edge effects are always present on non-spherical substrates. The non-uniform field around the edges would result in some degree of field enhancement. This is an area requiring further experimental investigation, particularly the degree of enhancement and its directional effect. Experimental observation also showed that particles bypassing the substrate initially could be deposited at the back of the object (known as wrap-round in EPC). The calculation model needs to be further extended to include the modelling of this back coverage phenomenon. The electrostatic forces responsible for this wrap-round process are still not clearly identified.

Figure 13 shows some experimental particle velocity distributions for 105–125 μm particles. Nearly all the recorded trajectories showed acceleration near the object, corroborating the experimental evidence (Corbett 1972) of field enhancement in the vicinity of the object. Whilst it

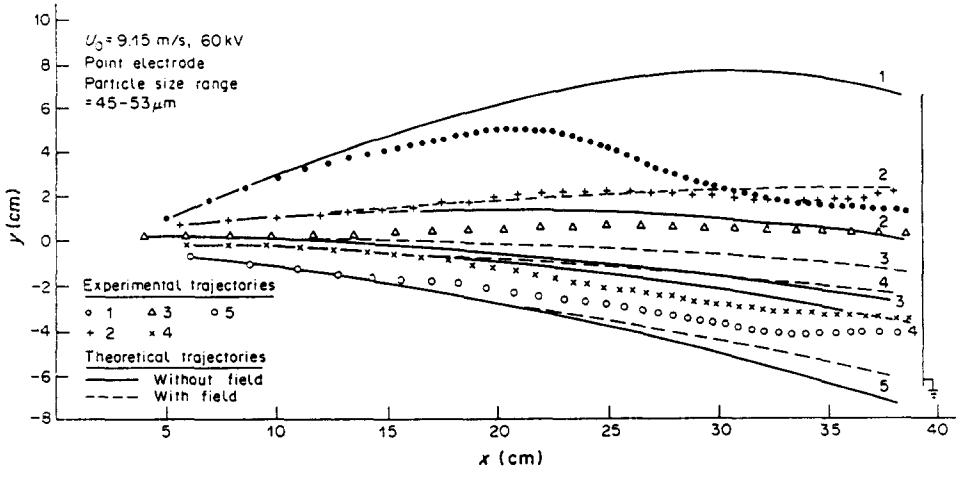

Figure 12. Comparison between experimental and theoretical trajectories.

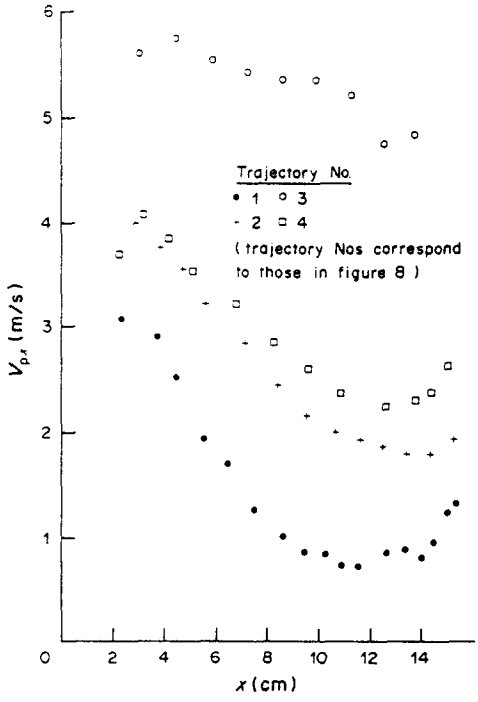

Figure 13. Experimental particle velocity distribution. V_{px} is the particle velocity in the x direction.

was difficult to determine the exact contribution to the particle velocity due to the electrostatic forces, it could be concluded that the air flow from the spraying device was responsible for conveying the particles to the object but the electrical forces dominated near the object and controlled the deposition process. Comparison between experimental and calculated particle velocities for some trajectories are shown in figures 14 and 15. The particle velocity component

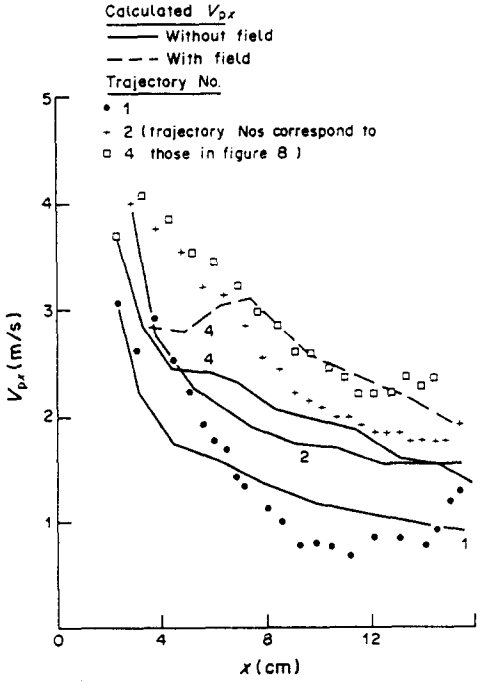

Figure 14. Comparison of experimental and calculated particle velocities.

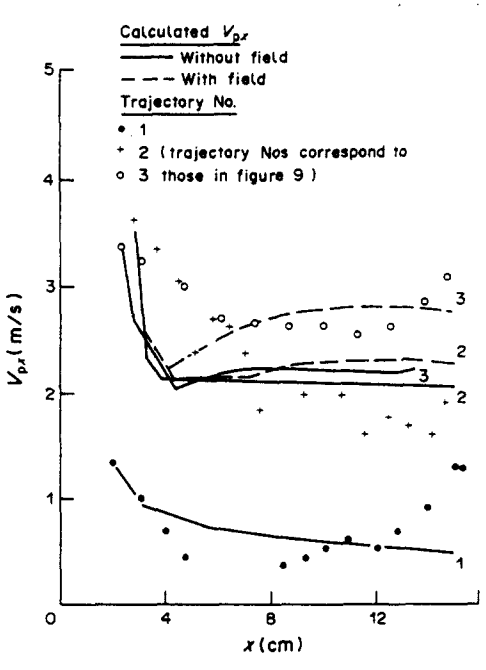

Figure 15. Comparison of experimental and calculated particle velocities.

contributed by the electrical fields was calculated to be of the order of 0.5–1.0 m/s. By adopting the criterion given by [19], the space charge effect was neglected in the calculation. The particle acceleration near the object was therefore not predicted. This criterion requires further evaluation. The predicted data also invariably displayed an initial sudden particle deceleration. This is due to the modelling deficiency in the description of the air flow between the electrode and the fully developed jet region. As shown in figure 5, the presence of a small electrode in the jet initial region resulted in a shift of the virtual source of the jet and also gave rise to a region of increasing fluid velocity before the fully developed flow region. In the prediction scheme a very simple velocity expressions, derived from the measurement of the centreline velocities, was adopted. The trajectory prediction could be considerably improved if a better model of the air velocity distribution for this region could be obtained.

Many of the present findings are consistent with the results of Abuaf & Gutfinger (1971, 1974). In their study excellent agreement was obtained, possibly because the experiments involved simpler geometry without the presence of an electrode in the jet stream. Furthermore, larger particles (250–417 μm) were used where the particle inertial effect would be predominant, and only selected particle trajectories that appeared to emerge from a common source were used for comparison.

The photographic technique has been shown to be an effective method for tracking charge particle trajectories, giving accurate data. It also yields interesting information on particle acceleration, wrap-round and the motion of particles in flight. The drawback of the technique is that it can be used only for very dilute suspensions.

5. CONCLUSIONS

Charged particle trajectories in EPC were measured experimentally and compared with theoretical predictions to evaluate the relative importance of the aerodynamic and electrostatic forces responsible for particle transport. It was shown that the air flow from the spraying device was responsible for the initial particle transport, with increasing dominance of electrostatic forces near the substrate mainly due to the field enhancement effect of the space charge. The various models describing these forces were compared, where possible, with experimental data and generally consistent agreement was obtained. The accuracy of prediction was found to depend on the initial particle exit position. Near the jet centreline the agreement was reasonable but away from it, the deviation became significant. Two possible sources of discrepancy could be poor prediction of particle drag force and inadequacy in modelling of the air flow field for the region between the electrode and the fully developed jet region. A further effect which could be significant but requires further investigation is the field enhancement at the edges of non-spherical objects.

Acknowledgements—The authors wish to express their gratitude to the Nordson Corporation (U.S.A.) and the consortium of 14 companies associated with the electrostatic powder coating industry for their financial support of this work.

REFERENCES

ABRAMOVICH, G. N. 1963 *The Theory of Turbulent Jets*. MIT Press, Cambridge, Mass.

ABUAF, N. & GUTFINGER, C. 1971 Entrainment of solid particles in a turbulent air jet—a preliminary study. *Israel J. Technol.* **9**, 389–395.

ABUAF, N. & GUTFINGER, C. 1974 Trajectories of charged particles in an air jet under the influence of an electrostatic field. *Int. J. Multiphase Flow* **1**, 513–523.

ANG, M. L. 1981 Trajectories of charged particles in electrostatic powder coating systems. Ph.D. Thesis, Loughborough Univ. of Technology, Leics.

BRIGHT, A. W. & BASSETT, J. 1975 Plant and equipment for the application of powder coatings. Presented at *Particle Wkshop on Electrostatic Powder Coating*, Chemical Engineering Dept, Loughborough Univ. of Technology, Leics.

CORBETT, R. P. 1972 A study of the electric fields and deposition process relevant to electrostatic powder coating. Ph.D. Thesis, Southampton Univ., Hants.

CROSS, J. & BASSETT, J. D. 1974 Observations during electrostatic deposition of high resistivity powders. *Trans. Inst. Metal Finish.* **52,** 112–113.

GOLOVOY, A. 1973a Deposition efficiency in electrostatic spraying of powder coating. *J. Paint Technol.* **45,** 42–48.

GOLOVOY, A. 1973b Particle deposition in electrostatic spraying of powder coatings. *J. Paint Technol.* **45,** 69–73.

HAKBERG, B., LUNGVIST, S., CARLSSON, B. & HOGBERG, T. 1983 A theoretical model for electrostatic spraying and coating. *J. Electrostat.* **14,** 255–268.

HARDY, G. F. 1974 Role of critical thickness in electrostatic powder deposition. *J. Paint Technol.* **46,** 73–82.

HARRIS, S. T. 1976 *The Technology of Powder Coatings.* Portcullis Press, London.

KORF, CHR. 1976 Powder coating—a report on materials, testing, plant and application. R. H. Chandler Ltd, Braintree, Essex.

SIBBETT, R. A. 1982 The effect of particle size on electrostatic powder coating. Ph.D. Thesis, Loughborough Univ. of Technology, Leics.

SINGH, S., O'NEILL, B. C. & BRIGHT, A. W. 1978 A parametric study of electrostatic powder coating. *J. Electrostat.* **4,** 325–334.

TING, Y. C. 1978 Back ionization in electrostatically deposited powder layers. M. Phil. Thesis, Southampton Univ., Hants.

WALLIS, G. B. 1969 *One-dimensional Two-phase Flow.* McGraw-Hill, London.

WHITE, H. J. 1963 *Industrial Electrostatic Precipitation.* Addison-Wesley, Reading, Mass.

WU, S. 1976 Electrostatic charging and deposition of powder coatings, *Polym.-Plast. Technol. Engng* **7,** 119–220.

YAMAMOTO, T. & VELKOFF, H. R. 1981 Electrohydrodynamics in an electrostatic precipitator. *J. Fluid Mech.* **108,** 1–18.